PCCP

PAPER

View Article Online
View Journal | View Issue

Cite this: *Phys. Chem. Chem. Phys.*, 2026, **28**, 288

A time-, angle- and kinetic-energy-resolved photoelectron spectroscopic study of tetrakis(dimethylamino)ethylene

Yuhuan Tian,†[ab] Zhichao Chen,†[a] Wenping Wu,[ab] Likai Wang,[ab] Zhigang He,[a] Dongyuan Yang,*[a] Guorong Wu*[a] and Xueming Yang[ac]

Received 5th October 2025,
Accepted 13th November 2025

DOI: 10.1039/d5cp03850b

rsc.li/pccp

The ultrafast electronic relaxation dynamics of tetrakis(dimethylamino)ethylene (TDMAE) following photoexcitation at ~267 nm is investigated using the time-, angle- and kinetic-energy-resolved photoelectron spectroscopy method, since we are motivated by the experimental findings in a previous similar study (E. Gloaguen *et al.*, *J. Am. Chem. Soc.*, 2005, **127**, 16529–16534). Based on the detailed analysis of the current high-quality data, the lifetime of the initially prepared ππ* state is found to be 50 ± 10 fs and it is clearly evident that an intermediate Rydberg state with a lifetime of 550 ± 50 fs plays a pivotal role in the photodynamics of TDMAE. In addition, a partial wave packet revival is also observed with a period of ~500 fs. This coherent oscillation, which is attributed to a vibrational quantum beat associated with overtones of the low-frequency C–C twist vibration in TDMAE, survives the ultrafast internal conversion processes and finally damps on a time scale of the order of several picoseconds.

1. Introduction

Time-resolved photoelectron imaging (TRPEI) is a widely employed methodology to investigate the excited-state nonadiabatic dynamics of gas-phase molecules from the time domain aspect, with emphasis on real time measurements of photoelectron spectra and angular distributions.[1–6] As we have already done, by combining a commercial Ti:sapphire femtosecond laser system and a velocity map imaging (VMI) spectrometer,[7] we have the capability of measuring the time-resolved photoelectron spectroscopy (TRPES) spectra along with the time-resolved photoelectron angular distributions (TRPADs) in a single pump–probe experiment, which allows us to study the ultrafast electronic relaxation dynamics of a series of isolated polyatomic molecules in more detail.[8–13] Here, we utilize VMI apparatus to perform a femtosecond TRPEI experiment of one specific substituted ethylene molecule, $[(CH_3)_2N]_2C{=}C[N(CH_3)_2]_2$, namely, tetrakis(dimethylamino)ethylene (hereafter termed simply TDMAE). Specifically, the ultrafast decay dynamics of TDMAE following photoexcitation at 266.9 nm is successfully explored.

TDMAE is one of the ethylene-like molecules with very low first adiabatic ionization potential (<5.4 eV),[14–16] while the corresponding difference between the adiabatic and vertical ionization potentials is ~0.8 eV. Soep *et al.* analyzed the time evolution of electronically excited TDMAE from the very initial excitation step down to the lowest fluorescence state, the charge transfer state, over widely different time scales.[17] The lifetime of the charge transfer state was measured to be ~22 ns. Later on, Soep and coworkers further studied the ultrafast electronic relaxation dynamics of this molecule by performing the TRPEI experiment.[18,19] Experimental evidence of the existence of a mediating state for the ultrafast electronic relaxation in TDMAE was found. In the present experimental study, we also obtain rich information about the radiationless decay mechanism in the UV-induced photodynamics of TDMAE, thanks to the ability of the TRPEI technique to efficiently extract TRPES and TRPAD data. Additionally, a vibrational quantum beat phenomenon was also clearly observed and reasonably explained. The detailed analysis of these data allows us to gain deep insights into the decay mechanism of electronically excited TDMAE.

2. Methodology

The TRPEI technology provides an opportunity to measure time-, angle- and kinetic-energy-resolved photoelectron spectroscopy

[a] *State Key Laboratory of Chemical Reaction Dynamics and Dalian Coherent Light Source, Dalian Institute of Chemical Physics, Chinese Academy of Sciences, 457 Zhongshan Road, Dalian, Liaoning 116023, China. E-mail: yangdy@dicp.ac.cn, wugr@dicp.ac.cn*
[b] *University of Chinese Academy of Sciences, Beijing 100049, China*
[c] *Department of Chemistry and Center for Advanced Light Source Research, College of Science, Southern University of Science and Technology, Shenzhen 518055, China*
† These authors made equal contributions.

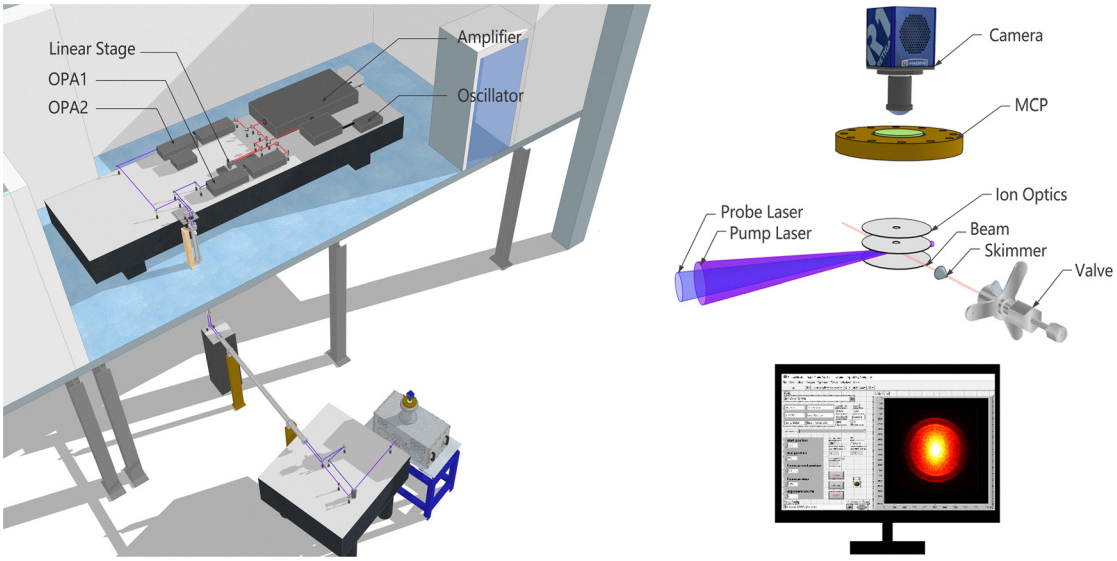

Fig. 1 Schematic view of the VMI spectrometer and the arrangement of the femtosecond laser system.

spectra.[20] To perform such experiments, we need to combine a VMI spectrometer with a femtosecond laser system, as shown in Fig. 1. A slightly more detailed description of the key features of the experimental method will be given in the following three sections since the present femtosecond TRPEI experiment was carried out on a newly constructed VMI spectrometer.

2.1 VMI spectrometer

The VMI spectrometer was recently constructed and very similar to our previous setup, as described in ref. 7. In brief, this apparatus consists of a source chamber and an interaction chamber, which are evacuated using a magnetically levitated turbo-molecular pump (Edwards, 3306c and 1003c) with pumping speeds of 3200 and a 1000 L s^{-1}, respectively, sharing a backing pump station (Edwards, T-station 85). The source and interaction chambers are separated by a skimmer (Beam Dynamics Inc., model 1). In the source chamber, a seeded TDMAE molecular beam was produced by expanding a mixture of sample vapor and helium carrier gas into the vacuum source chamber using a pulsed Even–Lavie valve operating at 1 kHz. Then, the supersonic jet-cooled molecular beam entered the interaction chamber through a 1 mm skimmer. In the interaction chamber, the pressure was maintained below 1×10^{-7} Torr throughout the experimental measurements.

The ion optics consists of three electrodes, namely, the repeller, extractor and ground electrodes.[21] All electrodes are 1-mm-thick stainless steel plates of diameter 56 mm mounted with aluminum oxide spacers of length 10 mm (Kimball Physics Inc.). The repeller electrode is a plate, while the hole at the center of the plate is 8 mm in diameter for the extractor electrode and 12 mm for the ground electrode. The electrons can be projected onto a 75-mm dual microchannel plate (MCP) detector backed by a P31 phosphor screen (Photonis, APD CT), which is recorded using a scientific camera (Teledyne Imaging, Retiga R1). The time-of-flight (TOF) axis is perpendicular to the plane containing the molecular beam and the laser beams. The ion optics and the TOF path to the detector are shielded from the stray electric and magnetic fields by a μ-metal shielding tube.

2.2 Ultrafast laser system

The femtosecond laser system used here is part of the ultrafast laser facility of the Dalian Coherent Light Source (DCLS). It consists of a fully integrated Ti:sapphire oscillator/amplifier system (Coherent, Legend Elite Duo) and two commercial optical parametric amplifiers (OPAs, Coherent, TOPAS Prime). The Legend Elite Duo delivers about 10 mJ per pulse at a laser repetition rate of 1 kHz from a regenerative amplifier stage plus single-pass power amplifier, with a pulse duration of ~35 fs and a central wavelength of ~800 nm. Both OPAs are pumped by a fraction (~2.7 mJ per pulse) of the fundamental 800 nm output. The outputs of OPAs are wavelength tunable and as short as 240 nm. In the present time-resolved study, 266.9 nm pump and the 387.9 nm probe laser pulses were generated from each OPA. The temporal delay between the pump and probe laser pulses was controlled by a linear stage (Newport, M-IMS400LM) located at the upstream of one of the OPAs. The pump and probe laser pulses were combined collinearly on a dichroic mirror without further compression and then focused using a calcium fluoride lens into the interaction region of the VMI spectrometer to intersect the seeded TDMAE molecular beam. All the femtosecond laser pulses were linearly polarized and the polarization direction was parallel to the MCP/phosphor screen detector. Electron kinetic energy calibration was achieved using multiphoton ionization of the Xe atoms.[7] In addition, the non-resonant two-color 1 + 3′ multiphoton ionization process of the Xe atoms was utilized to measure the time-zero and to estimate the 1 + 1′ cross-correlation between the pump and the probe laser pulse here.

2.3 Data acquisition program

We have developed an automated data acquisition program in the LabVIEW environment. The linear stage, the CCD camera and the optical shutters need to be controlled by this data acquisition program. This program also enables us to set parameters including the delays (equally or non-equally spaced) where the images are taken, the number of laser shots at each delay during delay scanning for the pump–probe signal and the number of delay scans. In the present measurement, a fine delay step of 25 fs was implemented. To minimize any small hysteresis effects, and the effects caused by the fluctuations and drifts in molecular beam intensity, laser pulse energy and pointing, *etc.*, the pump–probe time delays were scanned back and forth hundreds of times. Finally, the raw images for each delay were accumulated over approximately one million laser shots (several hundred[18] and ~5000[19] laser shots mentioned in the previous TRPEI experiments of TDMAE), enabling us to obtain high-quality TRPEI data for achieving the fast Fourier transform (FFT) of the oscillatory component and performing the reliable analysis of the energy- and time-dependent PADs. At the beginning and/or the end of each delay scanning, the background (time-independent) photoelectrons generated from single-color multiphoton ionization by each pump and probe laser beam can be recorded independently.

3. Results and discussion

In a specific pump–probe experiment, the TRPEI study of TDMAE upon femtosecond laser pulse excitation at 266.9 nm (a broad bandwidth with a full width at half-maximum (FWHM) of ~370 cm^{-1}) was performed. A combination of the TRPES and TRPAD data can provide rich useful information about the lifetime of each excited state, the decay channels and the coupling between the valence and Rydberg states. In the following sections, a detailed analysis and a reasonable interpretation of the TRPEI data will be given.

3.1 TRPES

In the TRPEI experiments, the raw 2D photoelectron images at selected pump–probe delays were recorded and transferred to 3D distributions using the pBasex Abel inversion method.[22] The time-dependent photoelectron 3D distributions were further integrated over the recoiling angle to derive the photoelectron kinetic energy distributions, *i.e.*, TRPES. In Fig. 2(a), the TRPES spectrum of TDMAE excited at 266.9 nm after subtracting the background photoelectrons generated from single-color multiphoton ionization is shown. Note that the energy axis is plotted in terms of electron binding energy of the excited state (hereafter termed simply binding energy), instead of photoelectron

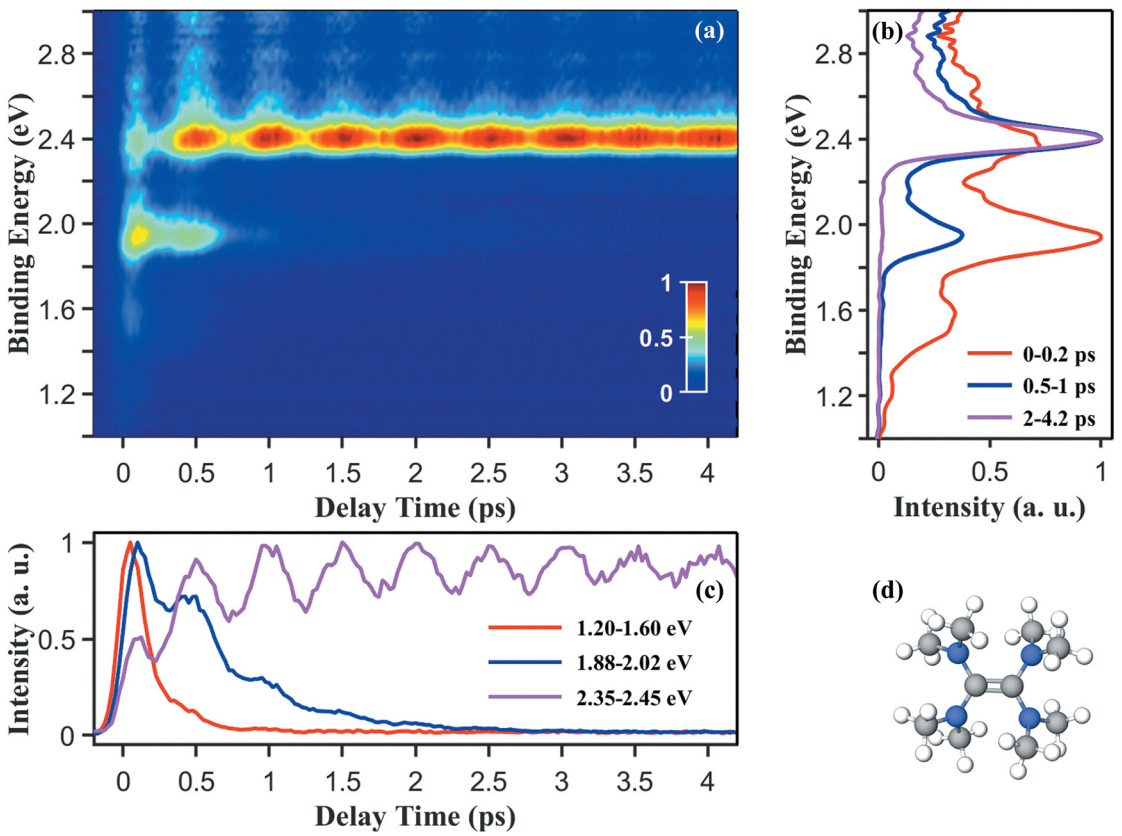

Fig. 2 (a) TRPES spectrum of TDMAE excited at 266.9 nm, after subtracting the background photoelectrons generated from single-color multiphoton ionization. Note that the energy axis is plotted in terms of electron binding energy of the excited state, instead of photoelectron kinetic energy. (b) Normalized electron binding energy distributions integrated over three selected pump–probe delay time ranges. (c) Normalized photoelectron transients integrated over three selected electron binding energy ranges. (d) A schematic structure of TDMAE.

kinetic energy. The electron binding energy distribution is associated with the character of the excited-state molecular orbital from which the electron is ionized, with respect to the electronic state of the cation that is left behind. Here, the binding energy distribution can be obtained by subtracting the measured photoelectron kinetic energy distribution from the single-photon energy of the probe laser. The TRPES spectrum of TDMAE (Fig. 2(a)) is only plotted in the 1.0–3.0 eV binding energy region. By visual inspection, it is obvious that the TRPES spectrum contains different components, each of which has a relatively strong peak centered at a specific binding energy and decays over different time scales, along with an oscillatory feature of the observed signal. The binding energy distributions over different delay ranges and the normalized transients over three binding energy ranges are presented in Fig. 2(b) and (c), respectively. A schematic structure of the TDMAE molecule is shown in Fig. 2(d).

In order to extract specific information, such as time constants and decay associated spectra (DAS), a 2D global least-squares method was employed to simultaneously fit the TRPES data at all delays and binding energies. The excited-state decay process can be described using the multi-exponential decay function along with an oscillatory component, as shown in the following expression:

$$\text{for } t \geq 0, I(t,\text{eBE}) = \sum_{i=1}^{n} \text{DAS}_i(\text{eBE}) \times \exp\left(-\frac{t}{\tau_i}\right) \times \left[1 + A_i \times \cos\left(\frac{2\pi t}{T} + \varphi_0\right) \times \exp\left(-\frac{t}{\tau_d}\right)\right]$$
$$\text{for } t < 0, I(t,\text{eBE}) = 0 \quad (1)$$

Herein, t is the pump–probe delay and eBE is the electron binding energy of the excited state. DAS_i(eBE) represents the decay associated spectrum associated with time constant, τ_i. $\cos(2\pi t/T + \varphi_0)$ represents the cosine function that describes the oscillatory nature of the signal, while T is the oscillating period and φ_0 is the initial phase. A_i represents the amplitude of the oscillatory component. This periodic modulation also needs to be described by a damped cosine function, $\cos(2\pi t/T + \varphi_0) \times \exp(-t/\tau_d)$, and τ_d is the damping time constant, denoting a dephasing of the coherence of the vibrational wave packet. Note that the experimentally observed pump–probe signal, $S(t)$, should be a convolution of a Gaussian cross-correlation function (*i.e.*, instrumental response function (IRF)) and the decay of the excited state population, $I(t)$.[23] As a consequence, the corresponding simulated 2D TRPES spectrum can be expressed as follows:

$$S(t,\text{eBE}) = I(t,\text{eBE}) \otimes \text{IRF} \quad (2)$$

Herein, the result of the convolution was obtained using a numerical convolution approach, which actually describes the relative detection efficiency of the excited state with a specific lifetime in a given time-resolved pump–probe measurement (*i.e.*, a given temporal profile of the corresponding IRF).[12,24,25] The 1 + 1′ IRF was estimated to be 150 ± 10 fs (FWHM) based on the approximation that both pump and probe laser pulses were a Gaussian profile. The time-zero and the 1 + 1′ IRF were varied in the range of their uncertainties to obtain a best fit.

A satisfactory 2D global least-squares fit to the TRPES spectrum (Fig. 2(a)) is achieved and the values of four different time constants (τ_1, τ_2, τ_3, and τ_4) together with their relative DAS are obtained, as shown in Fig. 3(a). The corresponding simulated 2D TRPES spectrum is plotted in Fig. 3(b). According to the analysis of the DAS, the feature of negative amplitudes clearly indicates that there exists a sequential kinetic process.[26,27] In the case of TDMAE, it is straightforward to assign the τ_1 time constant of 50 ± 10 fs to the lifetime of the initially prepared valence ππ* state ($C^{\bullet}$–$C^{\bullet}$ biradical type). At a pump wavelength of 266.9 nm, the ππ* state shows extremely fast decay dynamics, followed by the subsequent population of one specific π3p Rydberg state with a lifetime of 550 ± 50 fs (*i.e.*, τ_3). This short-lived intermediate Rydberg state further evolves to the long-lived zwitterionic state (C^{+}–C^{-}),[17] which decays in several 100 ps (τ_4, labeled as >100 ps in Fig. 3(a)) to the fluorescent charge transfer state (a positive charge located on one of the nitrogen atoms) with a lifetime of ~22 ns.[17] Since the charge transfer state was suggested to be 0.5 eV below the zwitterionic state,[16] at a probe wavelength of 387.9 nm (3.20 eV), the signal of single-photon ionization from the charge transfer state may appear in the very low photoelectron kinetic energy region and the photoionization cross-sections should be relatively weak (may be close to zero) due to the unfavorable Franck–Condon (FC) factor. We use the value of ~22 ns as the lifetime of the charge transfer state

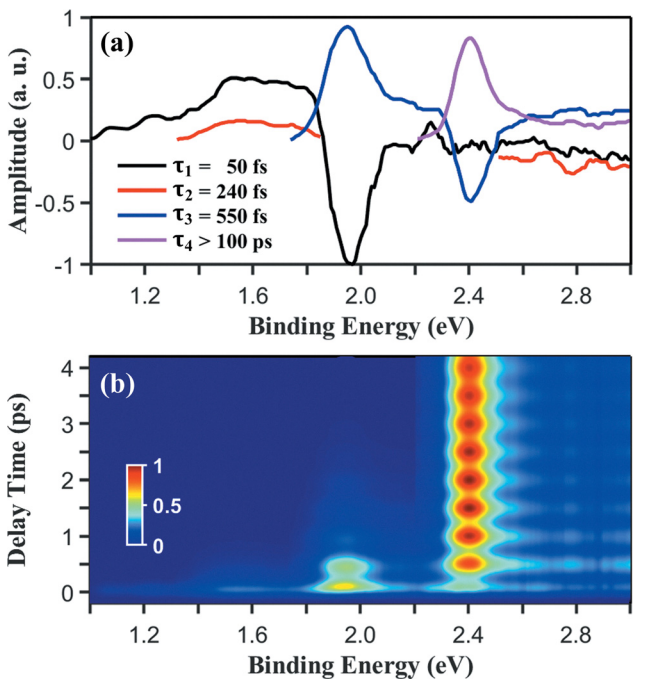

Fig. 3 (a) Decay associated spectra derived from a 2D global least-squares fit to the TRPES data shown in Fig. 2(a). (b) The corresponding fit to the experimental TRPES data.

hereafter. The above assignment of each time constant (τ_1, τ_3, and τ_4) is consistent with the previous similar TRPES study of TDMAE.[18,19]

However, the assignment of the τ_2 time constant is less clear-cut. A possible explanation is that the 240 fs component results from the pump–probe photoelectron signal of homoclusters. We note that the value of 240 ± 30 fs is in good agreement with the observed time constant in the TDMAE clusters.[28] Although we have confirmed that no $TDMAE_n^+$ ion clusters were detected in the time-of-flight (TOF) mass spectrum under our molecular beam conditions, the possibility of the influence of homoclusters still cannot be totally ruled out since TDMAE clusters might fragment upon photoionization before they arrive at the MCP detector of the VMI spectrometer. However, it should be mentioned that the contribution of the 240 fs component does not vary when the backing pressure of helium carrier gas was changed in a range of 1–5 bar. This also means that there is no evidence to support the existence of clusters in our present experimental measurements. Therefore, we prefer to speculate that this minor component of 240 ± 30 fs may be associated with another Rydberg state, presumably the $\pi 3d_{xz}$ state,[18] which is fairly close to the valence $\pi\pi^*$ state in TDMAE and is also directly excited at 266.9 nm. The deactivation pathway of the π3d Rydberg state is less clear-cut. Here, we tentatively propose that internal conversion to the nearby-lying valence $\pi\pi^*$ state is the dominant decay channel of the π3d state in TDMAE, the same as our previous explanation in the case of pyrrole.[13]

Note that the DAS of the τ_1 time constant has positive and negative values in different binding energy regions (see Fig. 3(a) and the equations in the SI). Additionally, the detection efficiency of the 50 ± 10 fs component is also relatively smaller than those of the other time constants (τ_2, τ_3, and τ_4, which are larger than 50 fs),[24] as shown in Fig. 3(a) and 4(a). Therefore, it should be pointed out that the major component of 50 ± 10 fs will be easily unobservable in the transients of the total photoelectron signal and the parent signal due to its small intensity in such transients. This is why the 50 ± 10 fs component was not observed in the previous femtosecond pump–probe experiments when monitoring the parent TDMAE molecule.[17,29]

3.2 Quantum beat

Apparently, an oscillatory feature can be observed in the present time-resolved pump–probe measurement, as shown in Fig. 2(a) and (c). The photoelectron transients show a very regular oscillation with a period of about 500 fs. All oscillations seem to be in phase (see Fig. S1 in the SI). The oscillatory component is described by a damped cosine function in combination with the exponential decay of the excited state population. As revealed by the result of the 2D global fit, the initial phase (φ_0) is zero and the oscillating period (T) is 500 ± 3 fs. In addition, the damping time constant (τ_d) is determined to be 3.0 ± 0.5 ps, which was not measured in the previous similar TRPEI experiments.[18,19] This dephasing lifetime should result from the intramolecular vibrational energy redistribution (IVR) process during the evolution of the vibrational wave packet on the excited-state potential energy surfaces (PESs). If the time constant of τ_d is not included in the fit (*i.e.*, $\tau_d = \infty$, $\exp(-t/\tau_d) \cong 1$), the fitting result will not be satisfactory, as revealed by the corresponding comparison (see Fig. S2 in the SI).

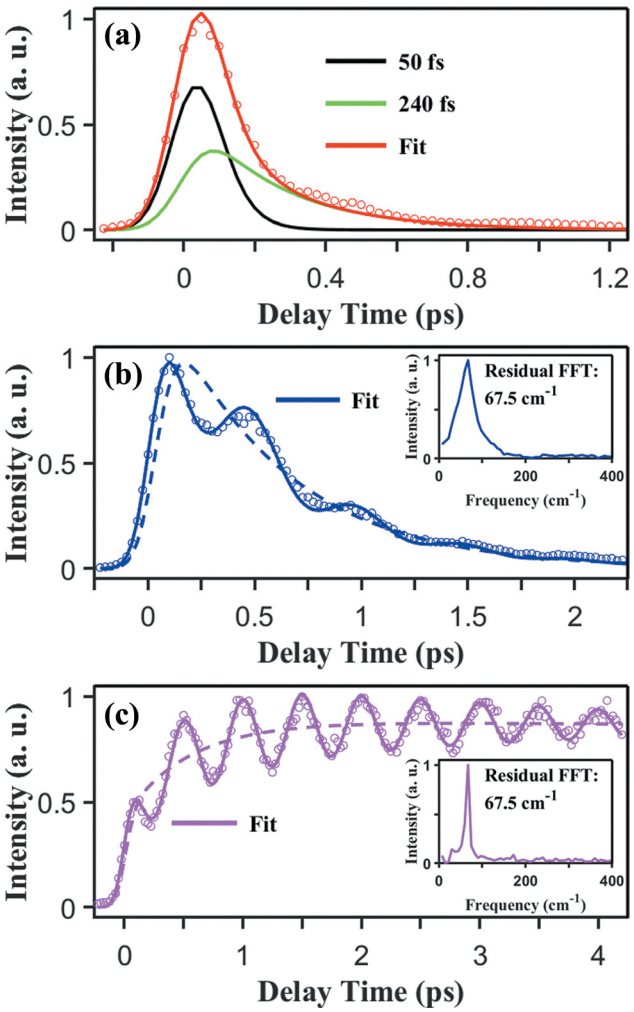

Fig. 4 (a) Normalized photoelectron transient derived by summing up the TRPES spectrum and the corresponding fit in the electron binding energy range of 1.20–1.60 eV. The cycles show the experimental data, while the solid lines show the fits. (b) and (c) The same as (a), but in electron binding energy ranges of 1.88–2.02 and 2.35–2.45 eV, respectively. In addition, the dashed line is the fit without the oscillatory component (see the main text for more details) and the inset shows the fast Fourier transform (FFT) of the oscillatory component.

Normalized photoelectron transients derived by summing up the measured TRPES spectrum (Fig. 2(a)) in electron binding energy ranges of 1.20–1.60, 1.88–2.02 and 2.35–2.45 eV are shown in Fig. 4(a), (b) and (c), respectively, while the fits to the experimental data are also included. In Fig. 4(b) and (c), the dashed line represents the fit without the oscillatory component (*i.e.*, $A_i = 0$ in eqn (1)). A fast Fourier transform was performed on the oscillating residuals,[30] as shown in the inset of Fig. 4(b) and (c). A frequency of 67.5 cm^{-1} (67.5 cm^{-1} is the peak position) dominates the Fourier spectrum (analysis in the frequency domain) which corresponds to a period of 494 fs.

As we know, the wave packet motion reflects the time evolution of a coherent superposition of the molecular system. In the case of TDMAE, the wave packet composed of two coherently excited vibrational states moves back and forth on the excited-state PESs, while the ionization probability varies accordingly due to the FC factor, which causes the modulation in the photoelectron transients. In the present time-resolved study, the experimentally observable signature of periodic modulation in the energy-resolved photoelectron transients should be due to a quantum beat involved with two vibrational states, the wavenumber separation of which is 67.5 cm^{-1}. We infer that the coherent superposition of combination modes involving the nv' and $(n + 2)v'$ vibrational states (here n is even and v' is the antisymmetric torsional mode of the central C–C bond in electronically excited TDMAE, with a low frequency of 67.5/2 cm^{-1}) causes the wave packet to move along the C–C torsional coordinate periodically, accompanied by a temporal modulation in the ionization probability associated with the ground state of the TDMAE cation ($D_0(\pi^{-1})$, which is significantly destabilized at a C–C twist of 90°). In other words, the D_0 state and the excited state (including the low-lying Rydberg state) PESs should not be entirely parallel to each other along the coordinate of oscillation (the C–C torsional coordinate is suggested here), which makes the observation of the present vibrational coherence possible. Actually, it is assumed to be approximately barrierless along the C–C torsional coordinate in the excited state PESs. In our opinion, the above explanation is also supported by the previous studies of quantum beat phenomena in ethylene[31] and ethylene-like molecules (*e.g.*, C_2F_4[32]). For the initially prepared electronic state(s), in the FC geometry where the ethylenic torsional angle is 0°, the ionization probability is maximal. In contrast, it is minimal when this torsional angle reaches 90° on the PESs of the initially and/or subsequently populated electronic states.

Although this wave packet composed of these coherently excited vibrational states is suggested to be formed in the initially prepared state(s), it should be pointed out that the oscillatory feature should not be obvious in the transient shown in Fig. 4(a) since the excited-state lifetimes of the initially prepared states are much lower than the oscillating period. The periodic modulation in the photoelectron transients shown in Fig. 4(b) and (c) should be mainly ascribed to the wave packet composed of the beating vibrational states on the PESs of the short-lived π3p Rydberg state and the long-lived zwitterionic state, respectively. Here, the frequency of this vibration is nearly identical on the π3p state and zwitterionic state surfaces, indicating that the zwitterionic state surface has almost the same curvature in the C–C twist direction as the π3p state surface, at least at early times before the depopulation of the subsequently populated zwitterionic state. This is also in reasonable agreement with the fitting result that there exists a similar modulation depth (~0.4) for all the observed oscillations (*i.e.*, $A_3 = A_4$ in eqn (1), see the SI for more details).

The vibrational quantum beat survives in the π3p state and the zwitterionic state since these electronic states are populated within the dephasing lifetime (3.0 ± 0.5 ps) of the coherence of the vibrational wave packet. In addition, the presently observed vibrational coherence corresponds to the oscillatory movement of the wave packet on a different coordinate (the C–C twist) nearly perpendicular to the evolution of the decay (such as the reaction coordinates involving the C–C stretch and some pyramidalization). Therefore, this coherent structural motion survives the population transfer between the electronic excited states. When the oscillating periods in all excited states are invariant here, the phase of the coherent oscillations is also retained before and after the internal conversion processes. Alternatively, we should expect a phase shift for the π3p and zwitterionic configurations, which is in contrast to the fact that all the observed oscillations have a regular initial phase of zero, as clearly illustrated in Fig. 2(c) and Fig. S1.

Herein our experimental findings confirm that the coherent torsional motion is preserved during the ultrafast internal conversion processes in TDMAE, strongly supporting the non-statistical nature of the internal conversion in the present case. This is also in good agreement with the conclusion in a previous experimental TRPES study on coherent structural dynamics after an internal conversion process in Rydberg-excited *N*-methyl and *N*-ethyl morpholine molecules.[33] Their important finding that the coherent motions persist well beyond electronic relaxation in the *N*-methyl morpholine system was further revealed by the time-resolved X-ray scattering measurement[34] and explained in depth in a number of recent studies.[35–38]

3.3 TRPADs

The TRPADs can be derived by integrating the 3D photoelectron distributions over a desired electron binding energy range. Here, the energy-dependent TRPADs were obtained over binding energy ranges of 1.20–1.60, 1.88–2.02 and 2.35–2.45 eV. These TRPADs can be further analyzed using the following expression for the (1 + 1′) two-photon ionization process with parallel linear polarizations:[39,40]

$$I(t,\theta) = \frac{\sigma(t)}{4\pi}[1 + \beta_2(t)P_2(\cos\theta) + \beta_4(t)P_4(\cos\theta)] \quad (3)$$

Herein, t is the pump–probe delay, $\sigma(t)$ is the time-dependent photoelectron signal and θ is the angle between the polarization direction of the pump and probe laser pulses and the recoil direction of the photoelectrons. $P_n(\cos\theta)$ terms denote the nth-order Legendre polynomials, while β_2 and β_4 are the well-known anisotropy parameters. For each delay and selected binding energy range, a satisfactory fit to the PAD was achieved and the values of anisotropy parameters were obtained.

The temporal evolution of the derived β_2 and β_4 anisotropy parameters as a function of pump–probe delay averaged over binding energy ranges of 1.20–1.60, 1.88–2.02 and 2.35–2.45 eV is plotted in Fig. 5(a), (b) and (c), respectively. In Fig. 5(a), the derived β_2 value is invariant with the change in the delay, with an average value of 0.72. The somewhat valence/Rydberg mixed character of the electronic configurations of TDMAE[18] reasonably explains why the derived β_2 value of the ππ* state is much

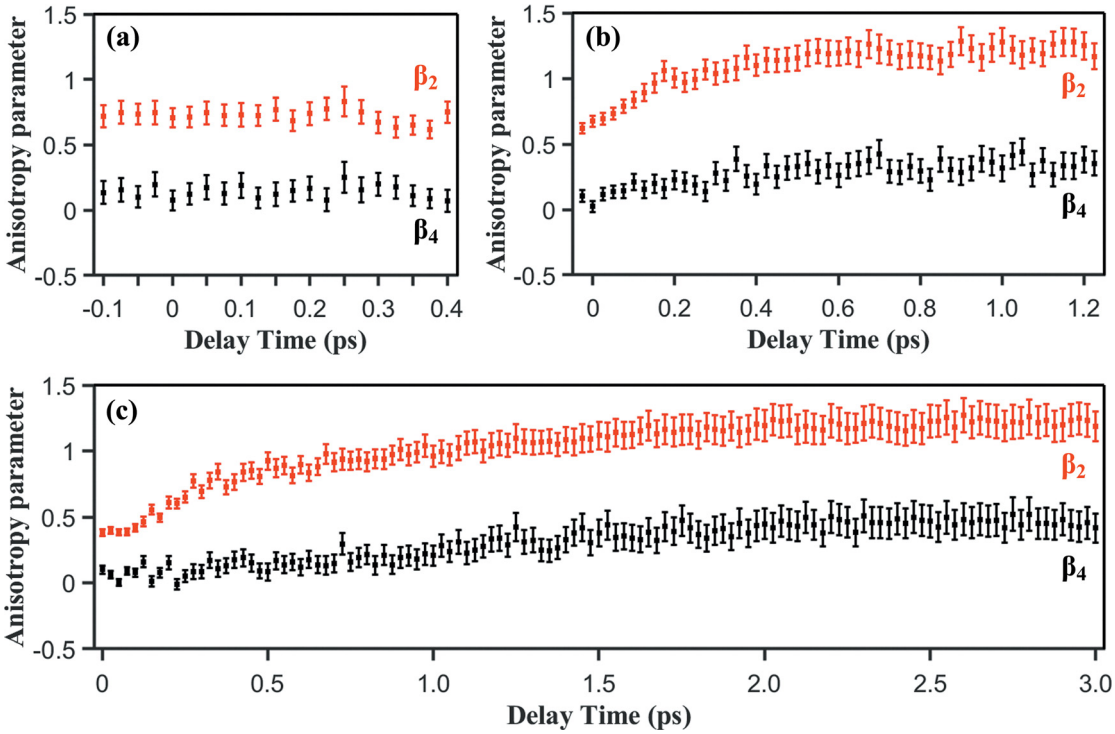

Fig. 5 (a) Temporal evolution of the β_2 and β_4 anisotropy parameters as a function of pump–probe delay averaged over the electron binding energy range of 1.20–1.60 eV. The error bars of the derived anisotropy parameters are also included. (b) and (c) The same as (a), but over electron binding energy ranges of 1.88–2.02 and 2.35–2.45 eV, respectively.

larger than zero. In Fig. 5(b), the derived β_2 value varies during the initial several hundred femtoseconds. This can be tentatively explained in terms of the overlap in the photoelectron signal (1.88–2.02 eV binding energy region) between the ππ* state and the intermediate Rydberg state. At larger delays, the average β_2 value is about 1.2, which is consistent with the expected value of an unpure π3p Rydberg state (probably the $\pi 3p_y$ state, as suggested by Soep *et al.*[18]). In Fig. 5(c), the derived β_2 value varies until about 1.5 ps, with a nearly invariant value of about 1.2 at delays larger than 1.5 ps. Interestingly, this reveals that the electronic character of the so-called zwitterionic state evolves differently from that of the population decay. One explanation is that there exists the coupling between the ππ* state and the zwitterionic state. When the unpure zwitterionic state is populated within about 1.5 ps, its electronic character changes from the partly ππ* to predominantly pure zwitterionic state, as revealed by the temporal evolution of the value of the β_2 anisotropy parameter shown in Fig. 5(c).

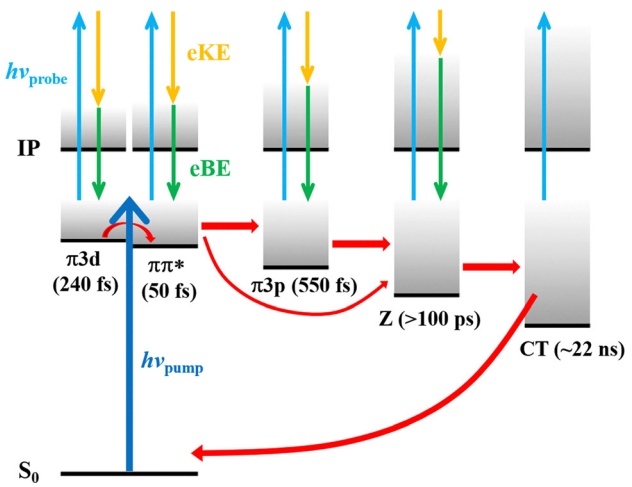

Fig. 6 Schematic representation showing the decay dynamics of the initially prepared excited states of TDMAE at a pump wavelength of 266.9 nm. Here, Z and CT represent the zwitterionic state and the charge transfer state, respectively.

3.4 Quantum yield of the intermediate Rydberg state

Based on the analysis of the experimental TRPEI data, a reasonable interpretation is proposed for the decay dynamics of the initially prepared electronic states of TDMAE at a pump wavelength of 266.9 nm, as summarized with a schematic view (Fig. 6). Both ππ* and π3d states are excited at 266.9 nm, with the contribution of the latter being minor (<15%, see the SI for more details). The decay channel of the π3d state is suggested to be internal conversion to the nearby-lying ππ* state, followed by the further deactivation of the ππ* state. There are two deactivation pathways of the valence ππ* state, which are as follows: ππ* → π3p → Z → CT → ground state and ππ* → Z → CT → ground state, while the excited-state lifetimes of ππ*, π3p, Z (zwitterionic state, C^+–C^-), and CT (fluorescent charge transfer state) are 50 fs, 550 fs, several 100 ps and ~22 ns, respectively. The estimated quantum yield of the intermediate

Rydberg state (*i.e.*, the branching ratio of $\pi\pi^* \rightarrow \pi 3p$) was determined to be 0.7 ± 0.1 based on the relative DAS (Fig. 3(a)) associated with τ_1 (50 ± 10 fs), τ_3 (550 ± 50 fs), and τ_4 (>100 ps), while the details have been given in the SI. Here, it should be mentioned that the photoionization cross-sections are assumed to be identical for the $\pi\pi^*$ state and the $\pi 3p$ state. According to the above quantum yield of 0.7, the decay rates of $\pi\pi^* \rightarrow \pi 3p$ and $\pi\pi^* \rightarrow Z$ can be calculated to be 1/71 fs^{-1} and 1/167 fs^{-1}, respectively.

4. Conclusions

In summary, we utilized a newly constructed VMI system in combination with tunable femtosecond laser pulses to explore the ultrafast excited-state decay dynamics of gas-phase molecules. In a femtosecond TRPEI experiment, the photodynamics of TDMAE excited at $\sim$267 nm was studied in more detail. By considering the coupling of the valence and Rydberg states in TDMAE, we propose a more comprehensive picture of the excited-state dynamics to reasonably explain the current experimental findings. In particular, the coherent torsional motion was found to be preserved during the ultrafast internal conversion processes, highlighting the non-statistical nature of internal conversion in the case of TDMAE.

Author contributions

Supervision and project administration: Dongyuan Yang, Guorong Wu and Xueming Yang; conceptualization: Dongyuan Yang and Guorong Wu; methodology: Yuhuan Tian, Zhichao Chen, Zhigang He, Dongyuan Yang and Guorong Wu; investigation and data curation: Yuhuan Tian, Wenping Wu and Dongyuan Yang; formal analysis: Yuhuan Tian, Wenping Wu, Zhichao Chen, Dongyuan Yang and Guorong Wu; discussion: all authors; writing: Dongyuan Yang and Guorong Wu; funding acquisition: Dongyuan Yang, Guorong Wu and Xueming Yang.

Conflicts of interest

There are no conflicts to declare.

Data availability

All data supporting the findings of this study will be available on reasonable request.

The details about the analysis of the pump–probe signals (the kinetic model associated with all excited states) and the damping of the oscillations, the TRPES spectrum at large delays and the measurement of the time-zero and cross-correlation have been given in the supplementary information (SI). See DOI: **https://doi.org/10.1039/d5cp03850b**.

Acknowledgements

This experimental work was financially supported by the National Natural Science Foundation of China (grant nos. 22203095 and 22288201), the Natural Science Foundation of Liaoning Province (grant no. 2025-BS-0148), the State Key Laboratory of Molecular Reaction Dynamics (grant no. SKLMRD-Z202406), the Dalian Institute of Chemical Physics (grant no. DICP I202304) and the Chinese Academy of Sciences (grant no. GJJSTD20220001). The authors also gratefully acknowledge the support and assistance from the Dalian Coherent Light Source (**https://cstr.cn/31127.02.DCLS**).

References

1 O. Gessner, A. M. D. Lee, J. P. Shaffer, H. Reisler, S. V. Levchenko, A. I. Krylov, J. G. Underwood, H. Shi, A. L. L. East, D. M. Wardlaw, E. T. Chrysostom, C. C. Hayden and A. Stolow, *Science*, 2006, **311**, 219–222.
2 C. Z. Bisgaard, O. J. Clarkin, G. Wu, A. M. D. Lee, O. Gessner, C. C. Hayden and A. Stolow, *Science*, 2009, **323**, 1464–1468.
3 T. Horio, T. Fuji, Y.-I. Suzuki and T. Suzuki, *J. Am. Chem. Soc.*, 2009, **131**, 10392–10393.
4 P. Hockett, C. Z. Bisgaard, O. J. Clarkin and A. Stolow, *Nat. Phys.*, 2011, **7**, 612–615.
5 N. Kotsina and D. Townsend, *Phys. Chem. Chem. Phys.*, 2021, **23**, 10736–10755.
6 D. Dowek and P. Decleva, *Phys. Chem. Chem. Phys.*, 2022, **24**, 24614–24654.
7 Z. He, Z. Chen, D. Yang, D. Dai, G. Wu and X. Yang, *Chin. J. Chem. Phys.*, 2017, **30**, 247–252.
8 D. Yang, Z. Chen, Z. He, H. Wang, Y. Min, K. Yuan, D. Dai, G. Wu and X. Yang, *Phys. Chem. Chem. Phys.*, 2017, **19**, 29146–29152.
9 W. Yuan, D. Yang, B. Feng, Y. Min, Z. Chen, S. Yu, G. Wu and X. Yang, *Phys. Chem. Chem. Phys.*, 2021, **23**, 17625–17633.
10 W. Yuan, B. Feng, D. Yang, Y. Min, S. Yu, G. Wu and X. Yang, *Chin. J. Chem. Phys.*, 2021, **34**, 386–392.
11 B. Feng, D. Yang, Y. Min, Q. Gao, B. Fang, G. Wu and X. Yang, *Phys. Chem. Chem. Phys.*, 2023, **25**, 17403–17409.
12 B. Feng, W. Wu, S. Yang, Z. He, B. Fang, D. Yang, G. Wu and X. Yang, *Phys. Chem. Chem. Phys.*, 2024, **26**, 8308–8317.
13 D. Yang, Y. Tian, Y. Min, Z. He, G. Wu and X. Yang, *Phys. Chem. Chem. Phys.*, 2025, **27**, 4467–4474.
14 Y. Nakato, M. Ozaki and H. Tsubomura, *Bull. Chem. Soc. Jpn.*, 1972, **45**, 1299–1305.
15 N. Mirsaleh-Kohan, W. D. Robertson, J. Lambert, R. N. Compton, S. A. Krasnokutski and D. S. Yang, *Int. J. Mass Spectrom.*, 2011, **304**, 57–65.
16 B. H. Smith and R. N. Compton, *J. Phys. Chem. A*, 2014, **118**, 7288–7296.
17 B. Soep, J. M. Mestdagh, S. Sorgues and J. P. Visticot, *Eur. Phys. J. D*, 2001, **14**, 191–203.
18 E. Gloaguen, J. M. Mestdagh, L. Poisson, F. Lepetit, J. P. Visticot, B. Soep, M. Coroiu, A. Eppink and D. H. Parker, *J. Am. Chem. Soc.*, 2005, **127**, 16529–16534.

19 E. Gloaguen, J. M. Mestdagh, L. Poisson, J. P. Visticot, B. Soep, M. Coroiu, A. Eppink and D. H. Parker, *AIP Conf. Proc.*, 2005, **762**, 869–874.
20 P. Trabs, F. Buchner, M. Ghotbi, A. Luebcke, H.-H. Ritze, M. J. J. Vrakking and A. Rouzee, *J. Phys. B: At., Mol. Opt. Phys.*, 2014, **47**, 124016.
21 A. Eppink and D. H. Parker, *Rev. Sci. Instrum.*, 1997, **68**, 3477–3484.
22 G. A. Garcia, L. Nahon and I. Powis, *Rev. Sci. Instrum.*, 2004, **75**, 4989–4996.
23 W. Wu, B. Feng, Y. Tian, Z. He, D. Yang, G. Wu and X. Yang, *J. Phys. Chem. A*, 2024, **128**, 8906–8913.
24 N. Kotsina and D. Townsend, *Phys. Chem. Chem. Phys.*, 2017, **19**, 29409–29417.
25 W. Wu, Y. Tian, Z. He, D. Yang, G. Wu and X. Yang, *Chin. J. Chem. Phys.*, 2024, **37**, 893–900.
26 G. Wu, A. E. Boguslavskiy, O. Schalk, M. S. Schuurman and A. Stolow, *J. Chem. Phys.*, 2011, **135**, 164309.
27 B. Feng, W. Wu, Z. He, D. Yang, G. Wu and X. Yang, *J. Phys. Chem. A*, 2024, **128**, 3840–3847.
28 S. Sorgues, J. M. Mestdagh, E. Gloaguen, J. P. Visticot, M. Heninger, H. Mestdagh and B. Soep, *J. Phys. Chem. A*, 2004, **108**, 3884–3895.
29 S. Sorgues, J. M. Mestdagh, J. P. Visticot and B. Soep, *Phys. Rev. Lett.*, 2003, **91**, 103001.
30 D. Yang, Y. Min, B. Feng, X. Yang and G. Wu, *Phys. Chem. Chem. Phys.*, 2022, **24**, 22710–22715.
31 T. Kobayashi, T. Horio and T. Suzuki, *J. Phys. Chem. A*, 2015, **119**, 9518–9523.
32 S. A. Trushin, S. Sorgues, W. Fuss and W. E. Schmid, *ChemPhysChem*, 2004, **5**, 1389–1397.
33 Y. Zhang, H. Jónsson and P. M. Weber, *Phys. Chem. Chem. Phys.*, 2017, **19**, 26403–26411.
34 B. Stankus, H. Yong, N. Zotev, J. M. Ruddock, D. Bellshaw, T. J. Lane, M. Liang, S. Boutet, S. Carbajo, J. S. Robinson, W. Du, N. Goff, Y. Chang, J. E. Koglin, M. P. Minitti, A. Kirrander and P. M. Weber, *Nat. Chem.*, 2019, **11**, 716–721.
35 M. D. J. Waters, A. B. Skov, M. A. B. Larsen, C. M. Clausen, P. M. Weber and T. I. Solling, *Phys. Chem. Chem. Phys.*, 2019, **21**, 2283–2294.
36 M. D. J. Waters, W. Du, A. M. Carrascosa, B. Stankus, M. Cacciarini, P. M. Weber and T. I. Solling, *J. Phys. Chem. Lett.*, 2021, **12**, 9220–9225.
37 R. Dsouza, X. X. Cheng, Z. Li, R. J. D. Miller and M. A. Kochman, *J. Phys. Chem. A*, 2018, **122**, 9688–9700.
38 W. Du, Y. Gao, B. Stankus, X. Xu, H. Yong and P. M. Weber, *Phys. Chem. Chem. Phys.*, 2021, **23**, 27417–27427.
39 K. L. Reid, *Annu. Rev. Phys. Chem.*, 2003, **54**, 397–424.
40 T. Suzuki, *Annu. Rev. Phys. Chem.*, 2006, **57**, 555–592.

